Civil and Sustainable Urban Engineering

Research Article
Volume 4(1), 2024, 1−19
https://doi.org/10.53623/csue.v4i1.391

Behaviour of Reinforced Concrete Slabs with Embedded Polystyrene Spheres

Jen Hua Ling*, Ji Wei Lau, Yong Tat Lim

Centre for Research of Innovation & Sustainable Development, School of Engineering and Technology, University of Technology Sarawak, 96000 Sibu, Sarawak, Malaysia

*Correspondence: lingjenhua@uts.edu.my

SUBMITTED: 31 December 2023; REVISED: 5 February 2024; ACCEPTED: 10 February 2024

ABSTRACT: Polystyrene spheres can be used to substitute concrete in reinforced concrete slabs. Despite the weight, the structural performance of the slab would also be affected. This study investigated the behaviour of slabs containing polystyrene spheres under loads. Six specimens were fabricated and tested under the four-point load setup. The parameters studied included the diameters of the polystyrene spheres and the spacing between them. The polystyrene spheres reduced the slabs' first crack load, stiffness, yield strength, and ultimate strength. The first crack, yield, and ultimate loads decreased by 22.3%, 2.1%, and 4.1%, respectively, when the polystyrene sphere's diameter increased from 75 mm to 125 mm. As the polystyrene spheres' spacing decreased from 50 mm to 10 mm, the first crack, yield, and ultimate loads dropped 14.2%, 9.2%, and 7%, respectively. Despite some limitations identified during the feasibility analysis, specimen SP3 was found feasible as a simply supported one-way spanning slab. In the specimen, the polystyrene spheres were 0.625 times the slab thickness in diameter and 2.5 times the concrete cover in spacing.

KEYWORDS: Reinforced concrete slab; polystyrene spheres; flexural behaviour; four-point load test; concrete replacement

1. Introduction

A reinforced concrete slab is a flat structural element made of concrete. It is one of the largest members of a structure [1-3]. It functions as the floors, ceilings, and roof decks, designed to resist loads acting perpendicularly to its surface. One issue with slabs is the high weight-to-strength ratio [4], putting extra loads on the beam, columns, and foundations. This leads to larger structural elements [1, 3], which is uneconomical. The weight of slabs can be reduced by removing concrete through the creation of voids or incorporating lightweight materials (Table 1). This approach is conceptually viable based on the bending theory of flexural members. The concrete in the tension region presumably conveys no load [5], yet it remains crucial as a stress transfer medium [6]. Complete removal of concrete would jeopardise the slab's structural stability. The materials used to substitute concrete included plastic, recycled plastic, high-density polyethene, polystyrene, industrial sponges, and paper tubes (Table 1). These materials are generally lightweight and easily accessible. They do not chemically react with concrete, absorb water, or deform during concrete casting [5].

Table 1. Previous studies of lightweight slabs.

Methods	Materials	Reference
Creating voids in slabs	High-density polyethylene (HDPE)	[1, 5, 7, 8]
	Plastic	[9-12]
	Glass fiber plastic	[3]
	Plastic/recycled plastic	[9, 13]
	Paper tube	[14]
	Polypropylene plastic/recycled polypropylene	[3, 23-25]
Embedding lightweight materials in slabs	Styropor / polystyrene	[8, 15-17, 21]
	Industrial sponge	[18]

Lightweight materials come in various shapes (Table 2), often larger than aggregate in concrete [17]. The most common shape is spherical. Sharp corners or edges should be avoided. The round corners and smooth edges prevent stress concentration [19-21], resulting in better structural performance [22].

Table 2. Shapes of void formers embedded in slabs.

Reference	Sphere	Cuboid	Cube	Donut	Ellipsoid	Cylinder	Mushroom	Tube
[1]	√							
[5]	√							
[7]	√							
[9]	√							
[10]	√							
[11]	√							
[13]	√							
[16]	√							
[17]	√							
[18]	√							
[12]	√				√			
[21]	√	√				√		
[23, 24]	√	√						
[8]	√		√					
[19]	√		√	√	√		√	
[15]		√						
[3]			√	√				
[25]				√				
[14]								√

Among previous studies, the concrete replacement rarely exceeded 30% [17, 22]. These slabs' performance is often inferior to that of a solid slab. Most of them can only retain roughly 90% of the strength of a solid slab [17]. This is due to the following reasons:

- The presence of voids in slabs disrupts the member's stress distribution. This makes the growth and enlargement of cracks notably fast [16].
- Removing concrete from slabs reduces the slab's moment of inertia [16, 26]. This affects the ability of the member to resist bending [26].
- The voids near the reinforcements remove the concrete around them. This reduced the bond strength [16].

Despite this, removing concrete from the slab can improve material efficiency [21, 22]. If properly designed, the strength-to-volume ratio of these slabs can exceed that of a solid slab [22, 27]. The strength-to-volume ratio is sometimes known as the strength-to-weight ratio. This is conditional on the homogeneity of the concrete. There emerges a critical inquiry into the potential for further optimisation of lightweight slabs. The observed limitations in performance raise questions about whether there are other factors constraining their overall performance. This underscores the need for investigation.

In this study, polystyrene spheres were used to substitute concrete in reinforced concrete slabs. The specimens were tested in the laboratory. The purpose was to investigate the slabs' behaviour. The effects of (a) the size of polystyrene spheres and (b) the spacing between the polystyrene spheres were studied. Finally, the feasibility of the slabs was evaluated. This study contributes insights into how the slabs' geometrical configuration impacts their structural performance. Furthermore, the proposed criteria for feasibility analysis in this study might serve as a guide for future research.

2. Materials and Methods

2.1. Specimens.

Six slab specimens were fabricated in the laboratory (Figure 1, Table 3). A solid slab served as the control specimen (i.e., CS). Polystyrene spheres were embedded in five test specimens (i.e., SP1 to SP5). For the parameters studied, the sphere's diameter, d_p, ranged between 75 mm and 125 mm, and the longitudinal spacing between the spheres, s_p, varied from 10 mm to 50 mm (Table 4).

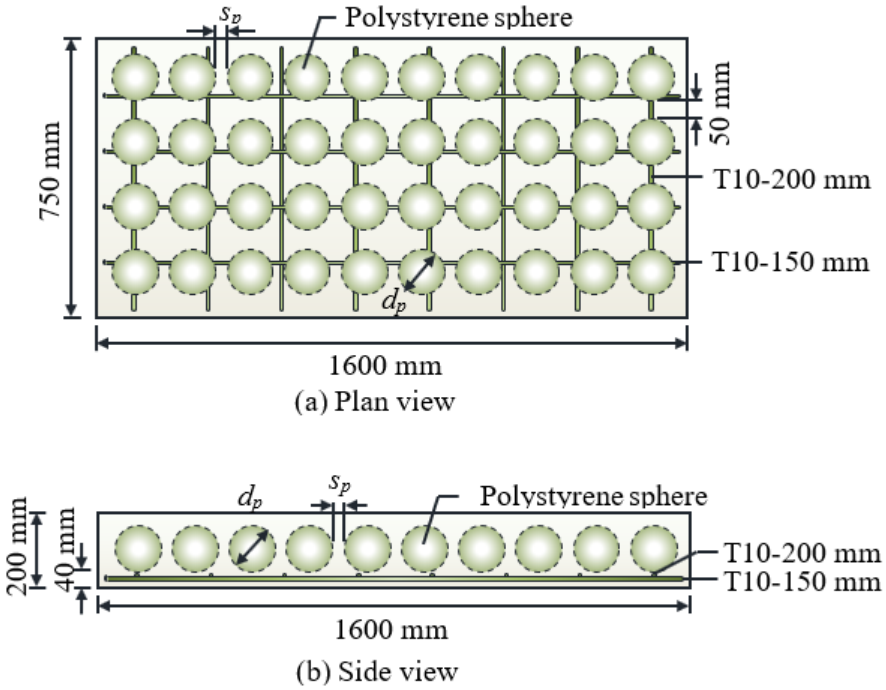

Figure 1. Details of test specimens.

Table 3. Details of specimens.

Details	Control specimen (CS1)	Test specimen (SP1 to SP5)
Dimension	750 mm in width, 1600 mm in length, and 200 mm in thickness	
Concrete	Grade C20/25, design slump = 100 mm to 180 mm, cover = 20 mm	
Reinforcement	High-strength steel bars with a nominal yield strength of 500 N/mm^2, bar diameter = 10 mm, spacing = 150 mm (main), 200 mm (secondary)	
Polystyrene spheres	Nil	Diameter = 75, 100, and 125 mm; longitudinal spacing = 10, 30, and 50 mm; transverse spacing = 50 mm; location = 40 mm from soffit

Table 4. Details of polystyrene spheres.

Type	Specimens	Changing Parameters		Nos. of polystyrene spheres
		d_p (mm)	s_p (mm)	$(n_l \times n_t = n_p)$
Control slab	CS 1	-	-	-
Slabs with polystyrene spheres	SP 1	75	50	12 × 6 = 72
	SP 2	100	50	10 × 5 = 50
	SP 3	125	50	9 × 4 = 36
	SP 4	125	30	10 × 4 = 40
	SP 5	125	10	11 × 4 = 44

d_p = diameter of polystyrene sphere; s_p = longitudinal spacing between polystyrene spheres; n_l = nos. of polystyrene spheres along the longitudinal section; n_t = nos. of polystyrene spheres along the transverse section; n_p = total nos. of polystyrene spheres in the specimen.

The specimens were cast in formworks made of 12 mm 3-layer plywood and 46 mm x 24 mm hardwood (Figure 2(a)). Steel reinforcements were prepared. The polystyrene spheres were tied together using galvanised wires (Figure 2(b)). The formwork was painted with used oil for waterproofing before being filled with ready-mixed concrete. Curing involved spraying the specimens with water and covering them with plastic sheets. After 28 days of casting, the specimens were tested.

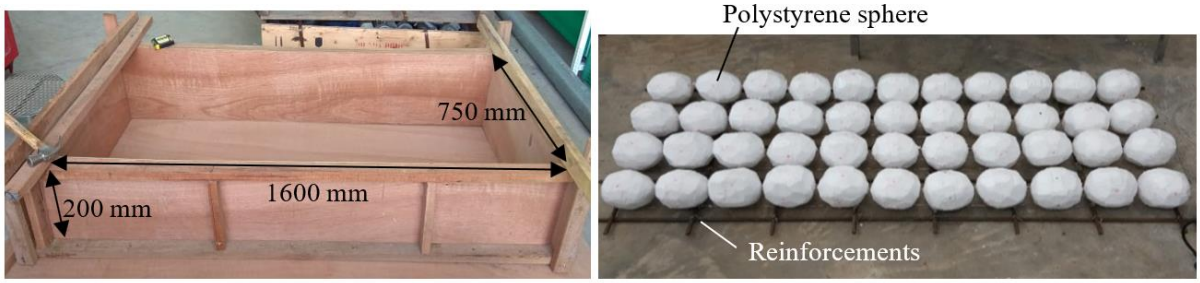

(a) Formworks (b) Reinforcement and polystyrene spheres

Figure 2. Preparation of specimen.

2.2. Test setup.

Each specimen was subjected to four-point load testing (Figure 3). The specimen was simply supported at a clear span of 1500 mm. A hydraulic jack was used to apply an incremental load to the specimen. Two steel rollers were then used to convert the load into two point loads at 260 mm spacing.

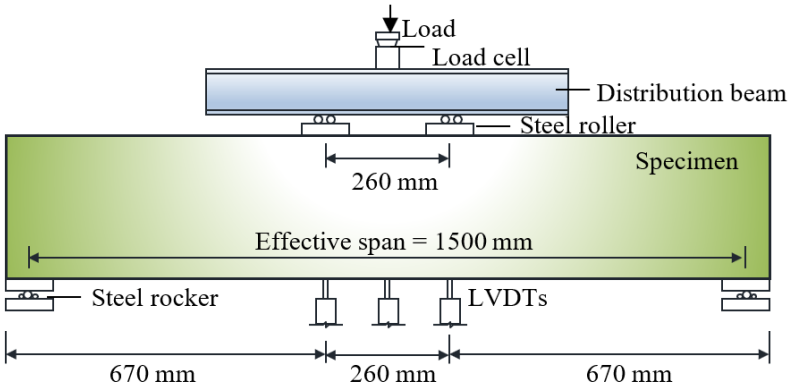

Figure 3. Test setup of specimen.

The measuring instruments included a load cell and three Linear Variable Differential Transformers (LVDT) (Table 5). The load cell was used to measure the load induced by the hydraulic jack. The LVDTs were utilised to measure the vertical displacement of the

specimen's soffit. One LVDT was installed in the midspan, and the other two were placed beneath the two point loads. All the measuring instruments were connected to a data logger for data acquisition.

Table 5. Test equipment and instruments.

Instrument	Model	Specifications	Accuracy
Hydraulic Jack	Enerpac RR-10018	933 kN load, 460 mm stroke, Double-Acting, Hydraulic Return	-
Hydraulic Pump	Enerpac P-462, Two-Speed Steel Hand Pump	700 bar operating pressure, 7423 cm^3reservoir capacity, 4,75 cm^3/stroke maximum flow at rated pressure	-
LVDT	TML CDP-100	100 mm stroke, 3 Hz frequency response, 0 to +40°C operating temperature	± 0.01 mm
Load Cell	TML CLJ-300KNB	Capacity 300kN, -20 to +70°C temperature range	± 0.1 kN
Data logger	TML TDS-630	50 Channels, speed 0.04 seconds/channel	0.1s measurement speed

2.3. Test procedure.

Before the test, a preload was applied to the specimen twice. The preload was approximately 10% of the specimen's estimated ultimate capacity. The load was held for 5 minutes before release. The specimen was left resting for 1 minute before the preload was applied again. The purposes of this process were to consolidate the test setup and check the measuring devices. Before the test began, all of the readings were reset to zero. The load was gradually increased. The load was held for at least 1 minute at every 5 kN or 0.5 mm, whichever came first. Then, readings were recorded, and the test proceeded. Throughout the test, the cracks on the specimen's surface were inspected. The test was stopped after at least three consecutive drops in the load measured.

3. Results and Discussion

3.1. Material properties.

The properties of the materials used in the specimens are given in Tables 6 and 7. The concrete met the designed cube strength of 25 N/mm^2. The reinforcements achieved the specified yield strength of 500 N/mm^2. Thus, the material quality was considered acceptable.

Table 6. Properties of concrete.

Specimen	Compressive Strength, f_{cu} (N/mm^2)		Average Compressive Strength, $f_{cu,\,avg}$ (N/mm^2)
	Cube 1	Cube 2	
CS 1	26.9	26.5	26.7
SP 1	26.4	26.0	26.2
SP 2	26.3	26.5	26.4
SP 3	26.4	25.7	26.1
SP 4	25.8	25.6	25.7
SP 5	25.2	25.2	25.2

CS = control slab, SP = slab with embedded polystyrene spheres.

Table 7. Properties of reinforcing steel.

Bar Diameter (mm)	Yield Strength, f_y (N/mm^2)			Average Yield Strength, $f_{y,avg}$ (N/mm^2)
	S1	S2	S3	
10	640	635	638	637.7

S1, S2 and S3 represented 3 different samples.

3.2. Geometrical properties.

The geometrical properties of the specimen can be represented by the ratios of sphere size, area replacement, volume replacement, and moment of inertia reduction: (Table 8)

a. The size of the polystyrene spheres may be expressed in a ratio, R_d, in a function of the polystyrene sphere diameter, d_p, and the slab's thickness, h:

$$R_d = \frac{d_p}{h} \quad (1)$$

where d_p = diameter of polystyrene sphere, mm; h = thickness of the solid slab, mm.

b. The area replacement ratio, R_a, resembles the effective concrete area of the slab's cross-section, A_s, relative to the cross-sectional area of the polystyrene spheres, A_p.

$$R_a = \frac{n_t \times A_p}{A_s} \quad (2)$$

where A_p = Cross-sectional area polystyrene spheres, mm^2; A_s = Cross-sectional area of a solid slab, mm^2; n_t = Number of polystyrene spheres in the transverse direction.

c. The volume replacement ratio, R_v, represents the effective concrete volume of the entire slab, V_s, compared to the volume of the polystyrene sphere, V_p.

$$R_v = \frac{n_p \times V_p}{V_s} \quad (3)$$

where V_p = total volume of polystyrene spheres, mm^3; V_s = volume of the solid slab, mm^3; n_p = total number of polystyrene spheres in the slab

The volumes of polystyrene spheres, V_p, and solid slab, V_s, are expressed in Eqs. 4 and 5, respectively.

$$V_p = \frac{1}{6}\pi {d_p}^3 \quad (4)$$

where d_p = diameter of polystyrene spheres, mm.

$$V_s = b \times h \times l \quad (5)$$

where b = width of the solid slab, mm; h = thickness of the solid slab, mm; l = length of the solid slab, mm.

d. The moment of inertia reduction ratio, R_i, is given in Eq. 6.

$$R_i = 1 - \frac{I_{eff}}{I_s} \quad (6)$$

where I_{eff} = effective moment of inertia of slab with polystyrene spheres, mm^4, I_s = moment of inertia of solid slab, mm^4

The effective moment of inertia of the slab with polystyrene spheres is given as:

$$I_{eff} = \sum\left(I_i + A_i {d_y}^2\right) \quad (7)$$

where I_i = moment of inertia of an area, mm^4; A_i = area of a shape, mm^2; d_y = distance between the area centroid and the slab's centroid.

The moment of inertia for the solid slab, I_s, and the polystyrene spheres, I_p, are given in Eqs. 8 and 9, respectively.

$$I_s = \frac{bh^3}{12} \quad (8)$$

$$I_p = \frac{\pi {d_p}^4}{64} \quad (9)$$

where b = width of the solid slab, mm; h = height of the solid slab, mm; d_p = diameter of polystyrene sphere, mm.

Table 8. Geometrical properties.

	Size ratio, R_d	Area of polystyrene spheres, A_p (mm^2)	Area replacement ratio, R_a	Volume of polystyrene sphere, V_p (mm^3)	Volume replacement ratio, R_v	Effective moment of inertia, I_{eff} (mm^4)	Moment of inertia reduction ratio, R_i
Ref.	Eq. 1		Eq. 2	Eq. 4	Eq. 3	Table 9	Eq. 6
SP 1	0.375	4,418	0.177	220,893	0.066	496,142,400	0.008
SP 2	0.500	7,854	0.262	523,599	0.109	494,262,786	0.011
SP 3	0.625	12,272	0.327	1,022,654	0.153	487,932,312	0.024
SP 4	0.625	12,272	0.327	1,022,654	0.170	487,932,312	0.024
SP 5	0.625	12,272	0.327	1,022,654	0.187	487,932,312	0.024

Sphere's diameter, d_p, spacing between polystyrene spheres, s_p, nos. of polystyrene in the transverse direction, n_t, and total nos. of polystyrene spheres, n_p, refer to Table 4; Slab's width, b = 750 mm; slab's thickness, h = 200 mm; slab's length, l = 1600 mm; Cross-sectional area of solid slab, A_s = 150,000 mm^2; volume of solid slab, V_s = 240,000,000 mm^3 (Eq. 5).

Table 9. Computation of slab's effective moment of inertia.

	Ref.	Specimen				
		SP 1	SP 2	SP 3	SP 4	SP 5
I_p	Eq. 9	1,553,156	4,908,739	11,984,225	11,984,225	11,984,225
y_p		77.5	90.0	102.5	102.5	102.5
$\Sigma A_i y_i$		14,657,605	14,293,140	13,742,120	13,742,120	13,742,120
ΣA_i		145,582	142,146	137,728	137,728	137,728
$\bar{y}$		100.7	100.6	99.8	99.8	99.8
$d_{y,s}$		-0.7	-0.6	0.2	0.2	0.2
$d_{y,p}$		-23.2	-10.6	2.7	2.7	2.7
$A_s d_{y,s}^2$		73,500	54,000	6,000	6,000	6,000
$A_p d_{y,p}^2$		2,377,944	882,475	89,463	89,463	89,463
$I_s+A_s d_{ys}^2$		500,073,500	500,054,000	500,006,000	500,006,000	500,006,000
$I_p+A_p d_{y,p}^2$		3,931,100	5,791,214	12,073,688	12,073,688	12,073,688
I_{eff}	Eq. 7	496,142,400	494,262,786	487,932,312	487,932,312	487,932,312

[1]Annotations: I = moment of inertia, A = area, y = centroid, d_y = distance between the centroid of area and centroid of the slab, *eff* = effective, s = solid slab, p = polystyrene sphere; [2] Moment of inertia of solid slab, I_s = 500,000,000 mm^4, Centroid of the solid slab, y_s = 100 mm, the centroid of the slab with polystyrene spheres,

$$\bar{y} = \frac{\sum A_i y_i}{\sum A_i}$$

3.3. Load-displacement response.

Figure 4 shows the load-displacement responses of the specimens. In general, each specimen went through three major stages before reaching its load capacity. This included the elastic, plastic, and failure stages.

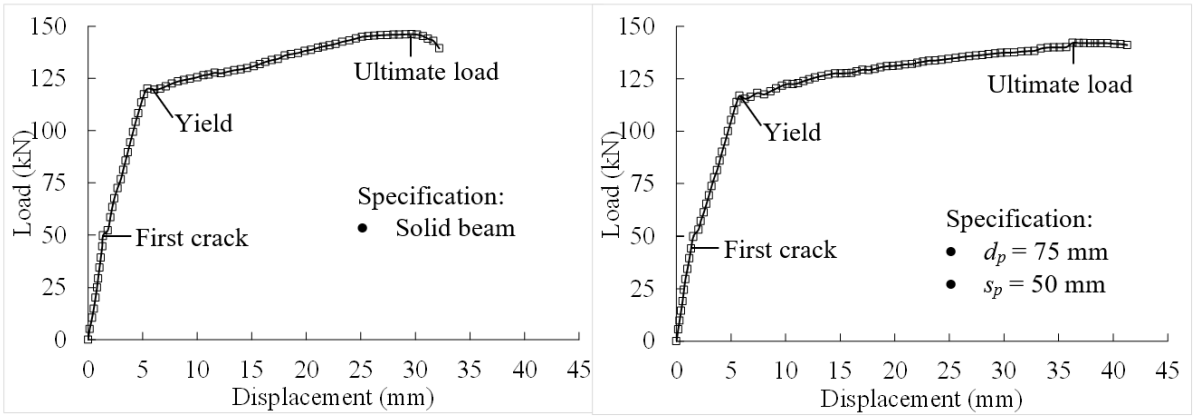

(a) Specimen CS1 (b) Specimen SP1

Figure 4. Load displacement response.

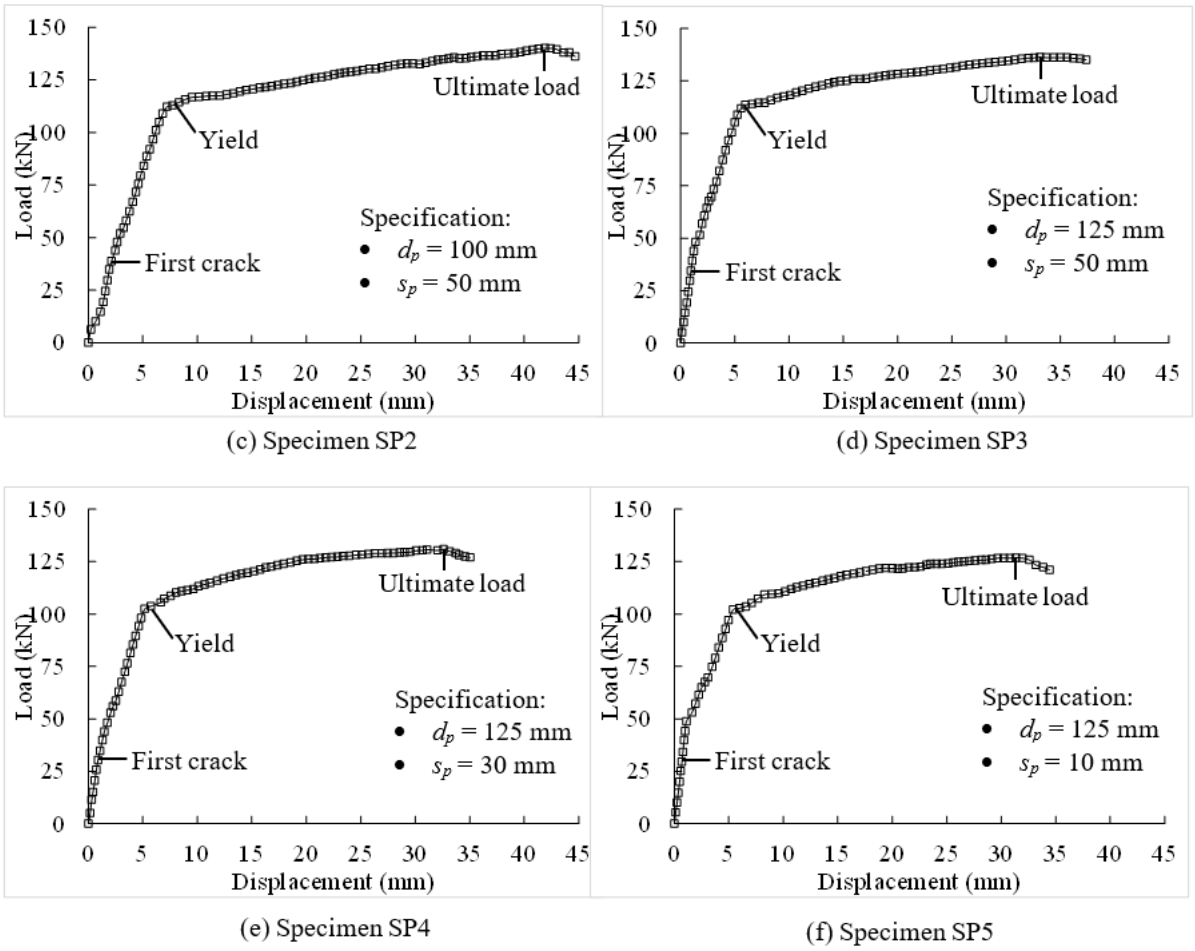

Figure 4. Load displacement response. (cont.)

The stiffness reflected the specimen's rate of deflection under load. The gradient of the load-displacement curve represented it. The uncracked stage had the highest stiffness. Upon entering the cracked stage, the stiffness reduced slightly. In the cracked stage, the deflection developed faster than in the uncracked stage. Before cracking, both the concrete and reinforcements resisted the flexural stress together. After the slab cracked, the concrete gave way, and the stress was fully taken by the reinforcements.

The yield point marked the end of the elastic stage. Then, plastic deformation began. The stiffness dropped dramatically, resulting in large deflections. This could be due to the yielding of steel reinforcement and the excessive cracking of concrete. The slab's integrity deteriorated gradually until critical damage appeared. The load peaked at the ultimate state, and thus the specimen was deemed failed.

3.4. Crack pattern and failure mode.

The load causes flexural stress near the slab's soffit. As a result, strains developed. Cracks formed when the strain exceeded the concrete's deformability limit. The cracks were predominantly flexural (Figure 5). The first crack appeared near the mid-span soffit. It began at the bar-concrete interface, subsequently spreading to the concrete surface [37]. The crack widened and penetrated deeper into the slab as the load increased. Then, more cracks appeared, and the cracked region widened. The cracks affected the bond between the concrete and the reinforcement. Excessive cracks deteriorated the composite action of the materials and affected

the slab's ability to carry the load [38]. This limited the load capacity of the specimen. Judging from the crack pattern, all the specimens failed in flexure.

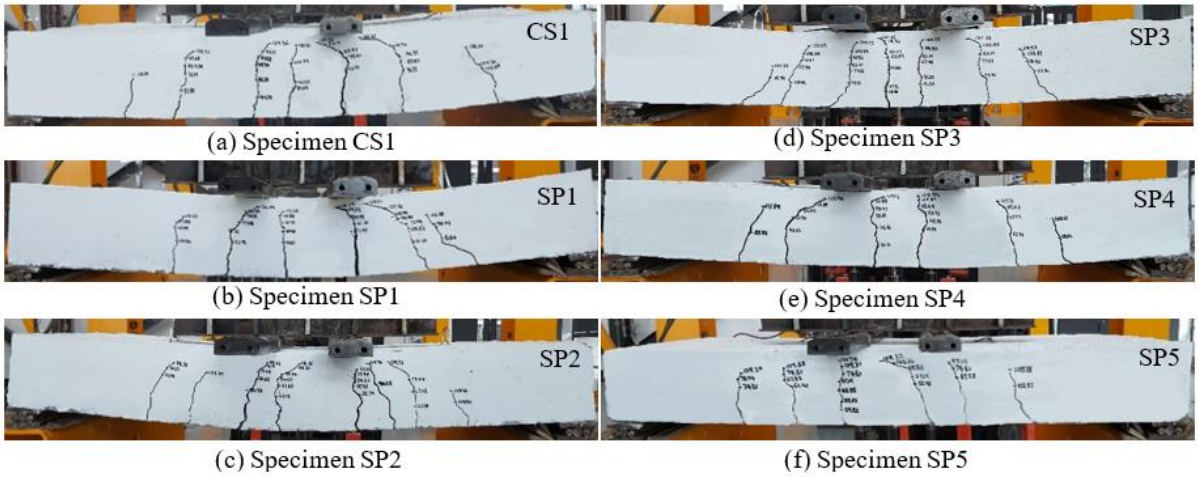

Figure 5. Crack pattern.

3.5. Test results.

Table 10 displays the specimen test results. This includes the specimens' properties at the elastic, yield, and ultimate stages. The results were computed based on Table 11.

Table 10. Test results.

Specimen	CS1	SP1	SP2	SP3	SP4	SP5
First crack load, P_{cr} (kN)	49.7	44.3	38.8	34.4	30.3	29.5
First crack displacement, δ_{cr} (mm)	1.36	1.34	2.12	0.96	0.89	0.70
Initial stiffness, S_i (kN/mm)	36.5	33.1	18.3	35.8	34.0	42.1
Secant stiffness, S_c (kN/mm)	23.4	20.9	16.1	21.2	20.2	19.6
Yield load, P_y (kN)	119.7	116.4	115.2	113.9	105.1	103.4
Yield displacement δ_y (mm)	6.25	6.8	8.7	6.43	6.48	6.47
Ultimate load, P_u (kN)	146.2	142.2	140.1	136.3	130.9	126.8
Ultimate displacement, δ_u (mm)	29.65	36.3	41.88	33.12	32.61	31.34
Ductility ratio, Δ	4.74	5.34	4.81	5.15	5.03	4.84

Table 11. Computation of slab's properties.

Results	Description
a. First crack load, P_{cr}	The load when the first crack was noticed. It was determined from Figure 5.
b. First crack displacement, δ_{cr}	The slab's deflection upon the first crack. It was obtained from the load-displacement curve in Figure 4.
c. Initial stiffness (uncracked), S_i	The stiffness of the specimen before cracking (Figure 6(a)). It was calculated by dividing the first crack load, P_{cr}, by the first crack displacement, δ_{cr}.
d. Secant stiffness, S_s	The stiffness represented the elastic response of the specimen. It was taken as the gradient of the line passing through the point of $0.75P_u$ (Figure 6(b)).
e. Yield point (P_y, δ_y)	The point when the specimen underwent plastic deformation. It was determined by using the method by Park (1988) [28] (Figure 6(b)).
f. Ultimate load, P_u	The largest load sustained by the specimen. It was determined from the peak of the load-displacement curve (Figure 4).
g. Ultimate displacement, δ_u	The deflection of the specimen corresponded with the ultimate load (Figure 4).
h. Ductility, Δ	The index implied the ductile behaviour of the specimen. It was computed by dividing the ultimate displacement, δ_u, by the yield displacement, δ_y.

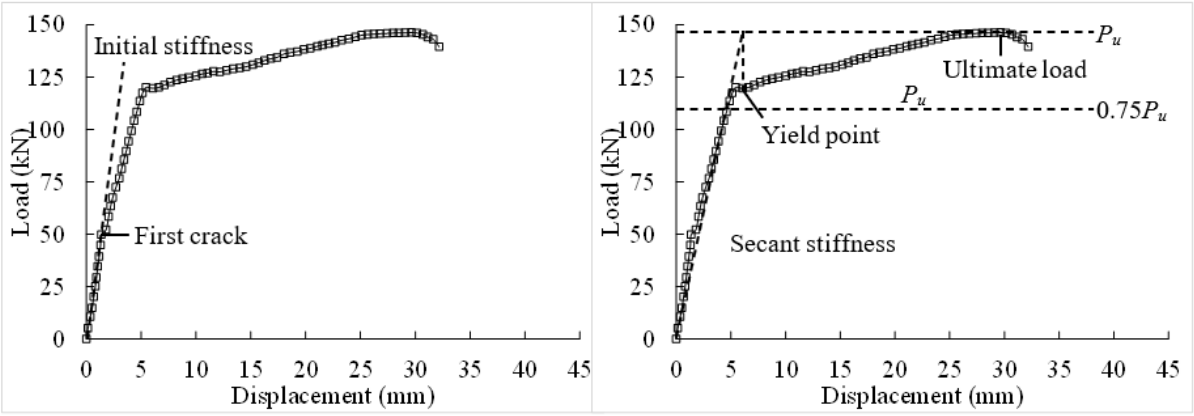

Figure 6. Methods to determine stiffness and yield point.

From Table 10, the following are observed:

- The first crack developed between 29.5 kN to 49.7 kN, which was equivalent to 23% to 34% of the specimens' ultimate loads.
- The specimens' stiffness before cracking (i.e. initial stiffness) was typically higher than their overall stiffness (i.e. secant stiffness).
- The specimens started experiencing plastic deformation between 103.4 kN and 119.7 kN. The yield load constituted about 80% to 84% of the specimens' ultimate loads.
- The specimens deflected considerably before failure. The ultimate displacement was 4.74 to 5.34 times the yield displacement. This can be observed from the ductility ratios.

To compare the test specimens (SP1 to SP5) with the control specimen (CB1), a series of performance ratios were generated (Table 12). The ratios were computed by dividing the properties of each test specimen by the control specimen.

Table 12. Performance of test specimens relative to the control specimen.

Specimen	Performance ratios					
	$\frac{P_{cr,i}}{P_{cr,c}}$	$\frac{S_{i,i}}{S_{i,c}}$	$\frac{S_{s,i}}{S_{s,c}}$	$\frac{P_{y,i}}{P_{y,c}}$	$\frac{P_{u,i}}{P_{u,c}}$	$\frac{\Delta_i}{\Delta_c}$
SP1	0.89	0.91	0.89	0.97	0.97	1.13
SP2	0.78	0.50	0.69	0.96	0.96	1.01
SP3	0.69	0.98	0.91	0.95	0.93	1.09
SP4	0.61	0.93	0.86	0.88	0.90	1.06
SP5	0.59	1.15	0.84	0.86	0.87	1.02

P_{cr} = first crack load, S_i = initial stiffness, S_s = secant stiffness, P_y = yield load, P_u = ultimate load, Δ = ductility ratio, i = test specimen, c = control specimen.

The polystyrene sphere negatively affected the overall structural performance of the slab. The slabs with polystyrene spheres (i.e., SP1 to SP5) generally had a lower first crack load, initial stiffness, secant stiffness, yield strength, and ultimate strength (Table 13). These properties were closely related to the slab's ability to withstand loads. Embedding polystyrene spheres in a slab altered its geometrical properties. As the size of the spheres increased, both the effective cross-sectional area and the sectional moment of inertia decreased. The reduced sectional area encouraged stress concentration in the slab. This led to the early development of the first crack. The smaller moment of inertia affected the slab's ability to resist bending. This reduced the slab's stiffness, yield strength, and ultimate strength.

Table 13. Effects of polystyrene spheres on slabs.

Effects of polystyrene spheres on:	Observations	Findings
a. First crack load	All specimens had the $\frac{P_{cr,i}}{P_{cr,c}}$ ratio less than 1.0.	The first cracks of the specimens developed earlier than the control specimen.
b. Initial stiffness	All specimens, except SP5, had the $\frac{S_{i,i}}{S_{i,c}}$ ratio less than 1.0.	The stiffness of the specimens at the uncracked stage was generally lower than the control specimen.
c. Secant stiffness	All specimens had the $\frac{S_{s,i}}{S_{s,c}}$ ratio less than 1.0.	The overall stiffness of the specimens at the elastic stage was lower than the control specimen.
d. Yield strength	All specimens had the $\frac{P_{y,i}}{P_{y,c}}$ ratio less than 1.0.	The specimens had lower design strength (i.e. yield strength) than the control specimen.
e. Ultimate strength	All specimens had the $\frac{P_{u,i}}{P_{u,c}}$ ratio less than 1.0.	The specimens had a smaller load capacity than the control specimen.
f. Ductility	All specimens had the $\frac{\Delta_i}{\Delta_c}$ ratio more than 1.0.	The specimens were more ductile than the control specimen.

The polystyrene spheres increased the slab's ductility slightly. This can be seen from the ratios $\frac{\Delta_i}{\Delta_c}$ of the specimens, which ranged from 1.01 to 1.13. The higher ductility was due to (a) lower stiffness, (b) smaller yield displacement, and (c) larger ultimate displacement of the slab. Polystyrene spheres affected the slab's ability to resist deformation. This encouraged the slab's deflection and caused it to enter the plastic stage early. For the lower slab's stiffness, the slab failed at the larger ultimate displacement. These combined effects resulted in a slightly higher ductility of the slab with polystyrene spheres.

3.6. Parametric responses.

The effects of the polystyrene sphere's size can be seen in specimens SP1, SP2, and SP3. The spacing between the polystyrene spheres in these specimens was set at 50 mm, which was 2.5 times the concrete cover. The slab's geometry changed as the size of the polystyrene sphere increased from 75 mm to 125 mm. Table 14 summarises how the changes affected the slab's structural performance. When the polystyrene sphere's diameter increased from 75 mm to 125 mm, (a) the first crack load decreased 22.3% from 44.3 kN to 34.4 kN, (b) the yield load dropped 2.1% from 116.4 kN to 113.9 kN, and (c) the ultimate load fell 4.1% from 142.2 kN to 136.3 kN (Table 10). These effects were in line with the implications identified from the geometrical changes of the specimen.

On the other hand, specimens SP3, SP4, and SP5 demonstrated the effects of spacing between the polystyrene spheres. In these specimens, the polystyrene sphere's diameter was fixed at 125 mm. Specimens SP3, SP4, and SP5 had a spacing of 50 mm, 30 mm, and 10 mm, respectively. The spacing imposed no geometrical changes to the slab's cross-section (Table 15). It only reduced the overall weight of the slab. Yet, the changes to the slab's structural performance were notable. As the polystyrene sphere's spacing decreased from 50 mm to 10 mm:

- The first crack load decreased 14.2% from 34.4 kN to 29.5 kN,
- The secant stiffness reduced by 8% from 21.2 kN/mm to 19.6 kN/mm,
- The yield load decreased by 9.2% from 113.9 kN to 103.4 kN,
- The ultimate load dropped 7% from 136.3 kN to 126.8 kN, and

- the ductility ratio reduced by 6% from 5.15 to 4.84.

Table 14. Effects of increasing the polystyrene sphere's diameter from 75 mm to 125 mm.

Observations from Table 8	Geometrical changes	Implications
a. The size ratio, R_d, increased from 0.375 to 0.625.	The polystyrene spheres occupied a space of around 37.5% to 62.5% of the slab's thickness.	i. A smaller space was available in the slab for laying the reinforcements. ii. Some parts of the secondary reinforcements were in direct contact with the spheres. This might affect the bond between the secondary reinforcement and the concrete.
b. The area replacement ratio, R_a, increased from 0.177 to 0.327.	17.7% to 32.7% of concrete in the slab's cross-section was replaced by polystyrene spheres.	i. A smaller effective area in the slab for stress distribution and absorption. ii. This led to the early formation of the first crack. iii. The shear strength of the slab may be impacted as well [1].
c. The volume replacement ratio, R_v, increased from 0.066 to 0.153.	6.6% to 15.3% of concrete volume was removed from the slab due to the substitution of polystyrene spheres.	i. Reduced the slab's overall weight. ii. This could improve the material's efficiency, resulting in greater strength per unit weight of the slab.
d. The moment of inertia reduction ratio, R_i, increased from 0.008 to 0.024.	The moment of inertia of the slab's cross-section was reduced from 0.8% to 2.4%.	i. Reduced the slab's ability to resist bending. ii. The slab's yield strength and ultimate strength were slightly affected.

[1] not investigated in this study.

Table 15. Effects of reducing the polystyrene sphere's spacing from 50 mm to 10 mm.

Observations from Table 8	Geometrical changes	Implications
a. The size ratio, R_d, of all specimens was 0.625 [1].	No change to the space in the slab's cross-section occupied by the polystyrene spheres.	No implication to the slab's structural performance from this aspect.
b. The area replacement ratio, R_a, remained constant, which was 0.327 [1].	No change to the percentage of concrete replacement in the slab's cross-section.	No effect on the slab's structural performance was expected from this.
c. The volume replacement ratio, R_v, increased from 0.153 to 0.187.	15.3% to 18.7% of the concrete volume being substituted by the polystyrene spheres.	Reduced the slab's overall weight.
d. The moment of inertia reduction ratio, R_i, was 0.024 throughout [1].	No change to the moment of inertia of the slab's cross-section.	No effects on the slab's bending resistance.

[1] The geometrical properties were based on the cross-section of the slab.

Polystyrene spheres removed concrete from the slab, creating elevated concrete sections in between, known as ribs (Figure 7). The ribs' width varied with the spacing between the spheres. Larger spacing meant wider ribs, making the lightweight slab stronger against load and deflection. Specimens SP3, SP4, and SP5 demonstrated increased ultimate load and secant stiffness as the spacing increased from 10 mm to 50 mm (Table 10). This was consistent with the findings of [33], and [34], confirming better specimen performance with larger ribs.

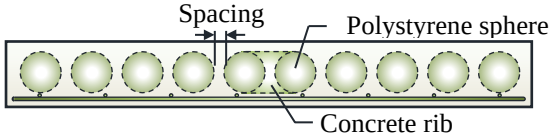

Figure 7. Concrete ribs between polystyrene spheres.

These ribs connected the top and bottom parts of the slab. Wider ribs strengthened the slab by providing a larger concrete cross-sectional area to distribute stresses. This minimised

localised high-stress points, which were vulnerable to cracking and failure. Additionally, wider ribs led to a larger cross-section and moment of inertia. This enhanced the slab's structural integrity, resulting in greater resistance to bending deformation and, thus, higher stiffness.

3.7. Feasibility Analysis

The slabs with polystyrene spheres were evaluated for feasibility in various aspects. It included the space occupied, weight reduction, material efficiency, load capacity, serviceability, ductility, and failure modes. The relevant criteria are outlined as follows:

a. C1: For a simply supported slab, only bottom reinforcements are required. The polystyrene spheres should not disturb the reinforcements, and adequate concrete cover should be maintained. The 20 mm concrete cover used in this study set a limit for the maximum size of the polystyrene sphere, $d_{p,lim}$ (Eq. 10). On this basis, the size ratio, R_{dp}, was preferably less than 1.0 (Eq. 11).

$$d_{p,lim} = h - 2c - d_{b,m} - d_{b,s} \tag{10}$$

$$R_{dp} = \frac{d_p}{d_{p,lim}} \leq 1.0 \tag{11}$$

where h = thickness of slab, mm, c = concrete cover, mm, $d_{b,m}$ = diameter of the main reinforcements, mm, $d_{b,s}$ = diameter of the secondary reinforcements, mm, d_p = diameter of polystyrene sphere, mm.

b. C2: The polystyrene spheres should replace a significant amount of concrete for a notable weight reduction [20]. While there is no set standard for the minimum percentage of replacement, the mean value of the specimens was used as a benchmark, as per [39]. Therefore, the preferred volume replacement ratio, R_v (see Table 8), was set to be at least the mean of all specimens, 13.7%.

c. C3: For effective usage of material, the strength per unit of concrete of the test specimen should be greater than that of the control specimen. Thus, the effective strength-volume ratio, R_e, should be at least 1.0 [27]. As all the test specimens met this requirement, a more rigorous passing criterion was applied, using the specimens' mean value as the benchmark.

$$R_e = \frac{E_{sp}}{E_s} \geq 1.074 \tag{12}$$

where E_{sp} = strength per unit concrete of the slab with polystyrene spheres, kN/m^3, E_s = strength per unit concrete of the solid slab, kN/m^3.

The strength per unit of concrete, E_{sp} and E_s, was determined by dividing the load capacity by the total concrete volume of the respective slab (Eq. 13 and 14).

$$E_{sp} = \frac{P_{u,sp}}{V_{sp}} \tag{13}$$

$$E_s = \frac{P_{u,s}}{V_s} \tag{14}$$

where $P_{u,sp}$ = ultimate load of the slab with polystyrene spheres, kN (Table 10); V_{sp} = concrete volume of the slab with polystyrene spheres, mm^3 (Eq. 15); $P_{u,s}$ = ultimate load of the solid slab, kN (Table 10); V_s = concrete volume of the solid slab, kN (Table 8).

$$V_{sp} = V_s - n_p V_p \quad (15)$$

where V_s = volume of the solid slab, mm^3 (Eq. 5); n_p = nos. of polystyrene spheres in the slab (Table 4); V_p = volume of a polystyrene sphere, mm^3 (Table 8).

d. C4: The slab with polystyrene spheres should have a larger load capacity than the solid slab. Thus, the strength ratio, R_s, should be at least 1.0.

$$R_s = \frac{P_{u,sp}}{P_{u,s}} \geq 1.0 \quad (16)$$

where $P_{u,sp}$ = ultimate strength of the slab with polystyrene spheres, kN; $P_{u,s}$ = ultimate strength of the solid slab, kN.

e. C5: The service load of the slab with polystyrene spheres should not be excessively low in comparison to its load capacity. Thus, the serviceability ratio, R_{sv}, should be at least 0.75 [29, 30].

$$R_{sv} = \frac{P_y}{P_u} \geq 0.75 \quad (17)$$

where P_y = yield strength of the beam with polystyrene spheres, kN; P_u = ultimate strength of the beam with polystyrene spheres, kN.

f. C6: The slab containing polystyrene spheres should be ductile enough for survival purposes. For use in low to moderate seismic zones, the ductility ratio, Δ, should be at least 4.0 [27, 29, 31-33].

$$\Delta = \frac{\delta_u}{\delta_y} \geq 4.0 \quad (18)$$

where δ_u = ultimate displacement of the beam with polystyrene spheres, mm; δ_y = yield displacement of the beam with polystyrene spheres, mm.

g. C7: The slab containing polystyrene spheres should perform comparable to a solid slab. One way to assess this was to examine if the failure mode was similar to that of a solid slab. Given the potential reduction in shear strength due to the polystyrene spheres, shear failure should be avoided. This condition applied provided that (a) the specimen was not subjected to excessive shear load and (b) the control specimen did not fail in shear.

Each specimen was evaluated based on criteria C1 to C7 (Table 16). None of the specimens fulfilled all the criteria. Thus, the specimens meeting the most criteria were identified. From the results, specimens SP3 and SP4 met all the criteria except C4. None of the specimens met the requirement of having an R_s greater than 1.0. This implied that the polystyrene spheres inevitably lowered the slab's ultimate strength.

Specimen SP3 performed better than Specimen SP4 in many aspects. It was (a) more efficient, offering a higher effective strength-to-volume ratio, R_e; (b) stronger, where the strength ratio, R_s, was greater; and (c) more ductile, where the ductility ratio, Δ, was higher. As a simply supported slab, specimen SP3 would be a preferable choice. In general terms, specimen SP3 had (a) the size of polystyrene spheres of 0.625 times the thickness of the slab and (b) the spacing between polystyrene spheres of 2.5 times the concrete cover.

Table 16. Feasibility analysis.

Criteria	Specimen	Ref.	SP 1	SP 2	SP 3	SP 4	SP 5	Mean
C1	Size ratio, R_{dp}	Eq. 11	0.54 √	0.71 √	0.89 √	0.89 √	0.89 √	
C2	Volume replacement ratio, R_v	Table 8	0.066 X	0.109 X	0.153 √	0.170 √	0.187 √	0.137
C3	Concrete volume of test specimen V_{sp} (mm^3)	Eq. 15	224,095,704	213,820,050	203,184,456	199,093,840	195,003,224	
	Strength per unit concrete, E (N/mm^3)	Eq. 13 & 14	0.0006346	0.0006552	0.0006708	0.0006575	0.0006502	
	Effective strength-volume ratio, R_e	Eq. 12	1.04 X	1.08 √	1.10 √	1.08 √	1.07 X	1.074
C4	Strength ratio, R_s	Eq. 16	0.97 X	0.96 X	0.93 X	0.90 X	0.87 X	
C5	Serviceability ratio, R_{sv}	Eq. 17	0.82 √	0.82 √	0.84 √	0.80 √	0.82 √	
C6	Ductility ratio, Δ	Table 10	5.34 √	4.81 √	5.15 √	5.03 √	4.84 √	
C7	Failure mode*[3]		F √	F √	F √	F √	F √	
	Score*[4]		3/6	4/6	5/6	5/6	4/6	
	Remarks*[5]		NA	NA	A	A	NA	

For CS1, V_{sp} = 240,000,000, E = 0.0006092, and Δ = 4.74; [1] Diameter of polystyrene sphere, d_p, refers to Table 4; Slab's thickness, h = 200 mm, Concrete cover, c = 20 mm, Size of reinforcements, $d_{b,m}$ and $d_{b,s}$ = 10 mm, Maximum allowable size of polystyrene sphere, $d_{p,lim}$ = 140 mm (Eq. 10); Ultimate load, P_u, and yield load, P_y, refer to Table 10; Volume of the solid slab, V_s = 240,000,000 mm^3; Volume of a polystyrene sphere, V_p, refer to Table 8; [2] √ - evaluation criteria met, X - evaluation criteria not met; [3] F – flexural failure; [4] Nos. of evaluation criteria met out of seven; [5] A – Applicable, NA – Not applicable

3.8. Limitations of study.

For simplicity, the weight and strength of polystyrene spheres were neglected. The space occupied by the polystyrene spheres was assumed to be stress-free voids. The volume of concrete replaced by the polystyrene spheres was thought to be proportionate to the weight decrease. This was provided that (a) the concrete was homogeneous throughout, and (b) the weight and strength of polystyrene spheres were minimal. No strain gauge was installed on the slab's reinforcements. It was hard to tell (a) if the reinforcements had yielded and (b) when they yielded. In this study, the reinforcements were believed to have yielded, based on the plastic deformation demonstrated in the slabs' load-displacement responses. The yield point identified from the load-displacement response was assumed to result from the yielding reinforcements.

The concrete strength of the test specimens was determined using concrete cubes cast alongside them. Presumably, homogenous concrete with an identical mix proportion, batch, and age would have the same strength. While this approach may not give an exact concrete strength, it is a common practice. The results served as a reference for checking the consistency and quality of the concrete. The test specimens were simply supported, one-way-spanning slabs, as evident from the setup using two rockers supporting the longer span. The test results may not fully capture the complex behaviour of two-way-spanning continuous slabs. For example, (a) the secondary reinforcement has a smaller impact on the flexural resistance of one-way spanning slabs than two-way spanning slabs, and (b) continuous slabs would

necessitate top reinforcements at the supports. Nonetheless, the study provides fundamentals, serving as a reference for further studies on two-way spanning slabs.

This study focuses on investigating the flexural behaviour of the lightweight slab. Removing concrete from a slab's cross-section reduces its effective shear area, making it more susceptible to shear load. One way to overcome this is to avoid replacing concrete in high-shear regions. Subsequent studies may explore the impacts of embedded lightweight materials on the slab's shear strength and ways to improve its shear resistance. The development of cracks was monitored through observation. However, there was a lag in crack detection. The internal cracks, which developed at the bar-concrete interface, were invisible until they were discovered on the concrete surface. By then, the internal cracks had already formed to a certain extent. Although the internal cracks were invisible, they changed the strain distribution in the bars and so affected the bond [37]. There was no explicit guide to evaluate the feasibility of the slabs. Seven evaluation criteria were established using the methodologies of earlier researchers [17, 29, 32, 34-36]. However, some constraints have been identified:

- The scope, number, and requirements of the criteria had a significant impact on the evaluation outcome. The selection outcome may differ if a different set of criteria is used. Therefore, the criteria used for the evaluation must be properly justified.
- The feasible and non-feasible specimens cannot be effectively distinguished using Criteria C1, C4, C5, C6, and C7. The criteria led to binary results where either all specimens passed or none did. As far as the current set of specimens was concerned, these criteria were redundant. Despite their limited utility in the current study, the criteria acted as a guide for future slab development.
- Criteria C2 and C3 set requirements based on the specimen group's mean values rather than theoretical benchmarks. This approach identified feasible specimens through relative comparisons among them. While not formally recognized by any standard, the two criteria played a pivotal role in this study's feasibility analysis.

4. Conclusions

The study examined the impact of varying sizes and spacings of embedded polystyrene spheres on the structural performance of reinforced concrete slabs. The conclusions are as follows:

- The structural performance of the slab was influenced by polystyrene spheres, resulting in reduced first crack load, stiffness, yield strength, and ultimate strength.
- As the polystyrene sphere's diameter increased from 75 mm to 125 mm, the first crack load, yield load, and ultimate load decreased by 22.3%, 2.1%, and 4.1%, respectively.
- When the spacing between polystyrene spheres decreased from 50 mm to 10 mm, the first crack load, yield load, and ultimate load decreased by 14.2%, 9.2%, and 7%, respectively.
- Specimen SP3 was found feasible as a simply supported one-way-spanning slab, meeting most evaluation criteria. It outperformed other specimens in various aspects, showcasing a more optimised design, with polystyrene spheres' diameter equal to 0.625 times the slab thickness and spacing equal to 2.5 times the concrete cover.
- The seven feasibility evaluation criteria employed in this study could potentially serve as a guide for future studies with a similar slab design.

Acknowledgements

This research work was funded by the Research Grants of University of Technology Sarawak UCTS/ RESEARCH/2/2018/02.

Competing Interest

The authors declare no conflict of interest.

References

[1] Bhade, B.G.; Barelikar, S.M. (2016). An experimental study on two way bubble deck slab with spherical hollow balls. *International Journal of Recent Scientific Research, 7(6)*, 11621−11626.

[2] Abg Adenan, D.S.Q.; Kartini, K.; Hamidah, M.S. (2020). Comparative study on bubble deck slab and conventional reinforced concrete slab – A review. *Journal of Advanced Research in Materials Science, 70(1)*, 18−26.

[3] Chung, J.H.; Choi, H.K.; Lee, S.C.; Choi, C.S. (2011). Shear capacity of biaxial hollow slab with donut type hollow sphere. *Procedia Engineering*, *14*, 2219–2222. https://doi.org/10.1016/j.proeng.2011.07.279.

[4] Yik, A.Y.M. (2021). Experimental and analytical study of the slab incorporating with lightweight material subjected to flexural and shear loads. Master thesis, University of Technology Sarawak, Malaysia.

[5] Ali, S.; Kumar, M. (2017). Analytical study of conventional slab and bubble deck slab under various support and loading conditions using Ansys Workbench 14.0. *International Research Journal of Engineering and Technology, 4(5)*, 1467−1472.

[6] Soji, S.; Anima, P. (2016). Experimental and analytical investigation on partial replacement of concrete in the tension zone. *International Journal of Engineering Research and General Science, 4(4)*, 23−32.

[7] Alfeehan, A.A.; Abdulkareem, H.I.; Mutashar, S.H. (2017). Flexural behavior of sustainable reactive powder concrete bubbled slab flooring elements. *Challenge Journal of Structural Mechanics, 3(2)*, 81−89. https://doi.org/10.20528/cjsmec.2017.04.010.

[8] Nimnim, H.T.; Zain Alabdeen, Z.M.J. (2019). Structural behavior of voided normal and high strength reinforced concrete slabs. *Kufa Journal of Engineering*, *10(2)*, 1−11. https://doi.org/10.30572/2018/KJE/100201.

[9] Oukaili, N.; Yasseen, H.H. (2016). Experimental investigations on the strength and serviceability of biaxial hollow concrete slabs. *Journal of Engineering, 22(11)*, 36−54. https://doi.org/10.31026/j.eng.2016.11.03.

[10] Raza, A.; Ahmad, M.E. (2021). Comparison of voided and solid reinforced concrete slabs. Proceedings of the 1st International Conference on Recent Advances in Civil and Earthquake Engineering, Peshawar, Pakistan.

[11] Schnellenbach-Held, M.; Pfeffer, K. (2002). Punching behavior of biaxial hollow slabs. *Cement and Concrete Composites, 24(6)*, 551−556. https://doi.org/10.1016/S0958-9465(01)00071-3.

[12] Ibrahim, A.M.; Ismael, M.A.; Abdul Hussein, H.A.S. (2019). The effect of balls shapes and spacing on structural behaviour of reinforced concrete bubbled slabs. *Journal of Engineering and Sustainable Development, 23(2)*, 56–65.

[13] Ibrahim, A.M.; Ali, N.K.; Salman, W.D. (2013). Flexural capacities of reinforced concrete two-way bubbledeck slabs of plastic spherical voids. *Diyala Journal of Engineering Sciences, 6(2)* 9−20. https://doi.org/10.24237/djes.2013.06202.

[14] Lee, C.H.; Mansouri, I.; Kim, E.; Ryu, J.; Woo, W.T. (2019). Experimental analysis of one-way composite steel deck slabs voided by circular paper tubes: Shear strength and moment–shear

interaction. *Engineering Structures, 182,* 227−240. https://doi.org/10.1016/j.engstruct.2018.12.063.

[15] Izzat, A.F.; Farhan, J.A.; Allawi, N.M. (2014). Behaviour and strength of one way reinforced concrete slabs with cavities. International Conference for Engineering Science At: Baghdad - University of Mustansiriyah.

[16] Al-Gasham, T.S.; Hilo, A.N.; M.A. Alawsi, (2019). Structural behavior of reinforced concrete one-way slabs voided by polystyrene balls. *Case Studies in Construction Materials, 11 (e00292),* 1−13. https://doi.org/10.1016/j.cscm.2019.e00292.

[17] Lau, J.W. (2021). Behaviour of lightweight reinforced concrete beam and slab system with embedded polystyrene spheres under flexural load. Master thesis, University College of Technology Sarawak, Malaysia.

[18] Jabir, H.A.; Jasim, M.; Al-Gasham, T.S. (2021). Conventional and bubble slab strips under limited repeated loads: A comparative experimental study. *Case Studies in Construction Materials, 14,* e00501. https://doi.org/10.1016/j.cscm.2021.e00501.

[19] Chung, J.H.; Park, J.H.; Choi, H.K.; Lee, S.C.; Choi, C.S. (2010).An analytical study on the impact of hollow shapes in bi-axial hollow slabs. Proceedings of Fracture Mechanics of Concrete and Concrete Structures - High Performance, Fiber Reinforced Concrete, Special Loadings and Structural Applications (FraMCoS-7).

[20] Lim, Y.T.; Ling, J.H.; Lau, J.W.; Yik, A.Y.M. (2021). Experimental study on the flexural behavior of reinforced polystyrene blocks in concrete beams. *Journal of the Civil Engineering Forum, 7(2),* 197−208. https://doi.org/10.22146/jcef.62346.

[21] Yik, A.Y.M.; Ling, J.H. (2020). Experimental study on voided slab subjected to flexural load. *Borneo Journal of Sciences and Technology, 2(1),* 27-31.

[22] Lim, Y.T.; Ling, J.H. (2019). Incorporating lightweight materials in reinforced concrete beams and slabs – A review, *Borneo Journal of Sciences and Technology, 1(2),* 16−26.

[23] Sagadevan, R. ; Rao, B.N. (2019). Experimental and analytical investigation of punching shear capacity of biaxial voided slabs. *Structures, 20,* 340−352. https://doi.org/10.1016/j.istruc.2019.03.013.

[24] Sagadevan, R. ; Rao, B. N. (2019). Effect of void former shapes on one‐way flexural behaviour of biaxial hollow slabs. *International Journal of Advanced Structural Engineering, 11,* 297–307. https://doi.org/10.1007/s40091-019-0231-7.

[25] Chung, J.H. ; Jung, H.S. ; Bae, B.i. ; Choi, C.S.; Choi, H.K. (2018). Two-way flexural behavior of donut-type voided slabs. *International Journal of Concrete Structures and Materials, 12,* 26. https://doi.org/10.1186/s40069-018-0247-6.

[26] Lim, Y.T.; Ling, J.H.; Lau, J.W.; Danson, T.T.L. (2021). Performance of reinforced concrete beam with polystyrene blocks at various regions. *Journal of Science and Applied Engineering, 3(2),* 62−71. https://doi.org/10.31328/jsae.v3i2.1655.

[27] Lau, J.W.; Ling, J.H.; Lim, Y.T. (2020). Feasibility study of reinforced concrete beam with embedded polystyrene spheres under incremental flexural load. *Borneo Journal of Science & Technology, 2(2),* 11−26.

[28] Park, R. (1988). Ductility evaluation from laboratory and analytical testing. The 9th World Conference on Earthquake Engineering, Tokyo-Kyoto, Japan, pp. 605−616.

[29] Ling, J.H.; Abd. Rahman, A.B.; Ibrahim, I.S.; Abdul Hamid, Z. (2017). An experimental study of welded bar sleeve wall panel connection under tensile, shear, and flexural loads. *International Journal of Concrete Structures and Materials, 11,* 525–540. https://doi.org/10.1007/s40069-017-0202-y.

[30] Ling, J.H.; Abd. Rahman, A.B.; Ibrahim, I.S. (2022). Deformation behavior of grouted sleeve wall connector under shear load in precast process of concrete wall. *Indonesian Journal of Computing, Engineering, and Design, 4(2),* 1−14. https://doi.org/10.35806/ijoced.v4i2.263.

[31] Soudki, K.A. (1994). Behaviour of horizontal connections for precast concrete load-bearing shear wall panels subjected to reversed cyclic deformations. PhD Thesis, University of Manitoba, Winnipeg, Manitoba.

[32] Ling, J.H.; Lim, J.H.; Abd. Rahman, A.B. (2021). Behaviour of precast concrete beam-to-column connection with SHS hidden corbel subjected to monotonic load. *Journal of the Civil Engineering Forum, 7(2),* 223−238. https://doi.org/10.22146/jcef.62930.

[33] Ling, J.H.; Abd. Rahman, A.B.; Ibrahim, I.S. (2014). Feasibility study of grouted splice connector under tensile load. *Construction and Building Materials, 50(1),* 530−539. https://doi.org/10.1016/j.conbuildmat.2013.10.010.

[34] Ling, J.H.; Lim, Y.T.; Leong, W.K.; Sia, H.T. (2021). Effects of adding silica fume and empty fruit bunch to the mix of cement brick. *Indonesian Journal of Computing, Engineering, and Design, 3(1),* 19−30. https://doi.org/10.35806/ijoced.v3i1.141.

[35] Ling, J.H.; Lim, Y.T.; Leong, W.K.; Sia, H.T. (2021). Utilization of oil palm empty fruit bunch in cement bricks. *Journal of Advanced Civil and Environmental Engineering, 4(1),* 1−10. https://doi.org/10.30659/jacee.4.1.1-10.

[36] Lim, Y.T. (2020). Performance of reinforced concrete beams with polystyrene as partial concrete replacement material under flexural loads. Master thesis, University College of Technology Sarawak, Malaysia.

[37] Pędziwiatr, J. (2008). Influence of internal cracks on bond in cracked concrete structures. *Archives of Civil and Mechanical Engineering, 8(3),* 91−105. https://doi.org/10.1016/S1644-9665(12)60165-4.

[38] Ling, J.H.; Ngu, J.T.S.; Lim Y.T.; Leong, W.K.; Sia H.T. (2022). Experimental study of RC hollow beams with embedded PVC pipes. *Journal of Advanced Civil and Environmental Engineering, 5(1),* 11−23. https://doi.org/10.30659/jacee.5.1.11-23

[39] Lim, Y.T.; Ling, J.H.; Sia, H.T.; Leong, W. K., Ngu, J.T.S. (2023). Improvement of reinforced concrete beam with embedded polystyrene under static load. *Indonesian Journal of Computing, Engineering, and Design*, 5(2), 67-77. https://doi.org/10.35806/ijoced.v5i2.331